JOURNAL OF CATALYSIS 150, 225–233 (1994)

Carbon-13 NMR Spectroscopy Study of L-Zeolite- and Silica-Supported Platinum Catalysts

S. B. Sharma,[1] T. E. Laska,[2] P. Balaraman, T. W. Root,[3] and J. A. Dumesic[3]

Department of Chemical Engineering, University of Wisconsin-Madison, Madison, Wisconsin 53706

Received January 18, 1994; revised August 1, 1994

NMR studies of CO adsorbed on small Pt particles show evidence of changes in the metallic nature of these particles with size. Large particles on silica or the exterior of zeolite crystallites have conduction-band electrons that cause a Knight shift for adsorbed CO. Small particles in zeolite cavities are diamagnetic clusters, and yield spectra for linear and bridging carbonyls similar to those of transition-metal cluster compounds. ^{13}C NMR of CO offers a simple probe of metal dispersion and particle size for these Pt catalysts and other noble metal systems. © 1994 Academic Press, Inc.

INTRODUCTION

Platinum particles supported on L-zeolite have been found to be active and selective for dehydrocyclization of normal paraffins (1–6), and these particles have also been suggested to possess unique chemisorptive properties (2, 7, 8). Spectroscopic studies have demonstrated that L-zeolite can stabilize cluster-sized platinum particles, consisting of 5–6 atoms, within the zeolite channels (9). Infrared spectroscopic studies (2, 8) of adsorbed CO have demonstrated that Pt/L-zeolite catalysts display additional infrared features which are unique to these materials, along with bands due to linear- and bridged-CO adsorption found for conventional supported platinum catalysts. These additional IR bands may be a consequence of the adsorptive properties of cluster-sized platinum particles (2) or they may be a result of interactions between the zeolite framework and the adsorbed CO (8).

In this paper, we report the results of ^{13}C NMR and IR spectroscopic studies of carbon monoxide adsorption on platinum particles supported on L-zeolite and amorphous silica. These spectroscopic techniques provide quantitative information on the distribution of the various types of adsorption sites. In addition, ^{13}C NMR gives information about the metallic character of the supported platinum particles through the Knight shift, which is caused by conduction–electron polarization at the Fermi level (10–13).

Well-resolved line shapes with chemical shifts typical of diamagnetic inorganic cluster compounds have been observed for CO adsorbed on highly dispersed rhodium and ruthenium (14–17). The metal particles on these supported catalysts are sufficiently small that they lack a fully developed conduction band, and the Knight shift is absent (18). Similar behavior has been observed for alkali-promoted Rh/SiO_2 catalysts (19). We show here that Pt clusters in L-zeolite do not give rise to a Knight shift for adsorbed CO. These results indicate that ^{13}C NMR can be used to distinguish cluster-sized platinum particles within the channels of L-zeolite from larger platinum particles that may be present on the external zeolite surface. Furthermore, the absence of a Knight shift for these cluster-sized platinum particles in L-zeolite allows ^{13}C NMR to be used to provide unique information about the nature of carbon-containing species on platinum surfaces. A related study (20) reports the use of ^{13}C NMR along with microcalorimetry and reaction kinetics to investigate the catalytic reactivity and deactivation behavior of Pt surfaces for *n*-hexane conversion.

EXPERIMENTAL

The Pt/K–L-zeolite and Pt/K(Ba)–L-zeolite catalysts used in this study were synthesized by Dr. J. T. Miller at Amoco. The L-zeolite support was obtained from Union Carbide. The zeolites were base-exchanged to full capacity and calcined at 823 K. Platinum was then incorporated into the zeolite by incipient wetness impregnation with an aqueous solution of $Pt(NH_3)_4(NO_3)_2$. Prior to use, the impregnated catalysts were calcined in air at 533 K for 3 h and reduced in hydrogen at 773 K for 2 h. The Pt/L-zeolite catalysts contain approximately 1% Pt by weight. A 4% Pt/SiO_2 catalyst was synthesized by the ion-exchange procedure of Benesi *et al.* (21). Prior to use, the dried catalyst was calcined at 548 K in flowing oxygen (60 cc/min) for 1 h and subsequently reduced at 673 K in

[1] Present address: Mobil Research & Development Corp., Central Research Laboratory, P.O. Box 1025, Princeton, NJ 08540.

[2] Present address: Procter and Gamble Company, 5299 Spring Grove Ave., Cincinnati, OH 45217.

[3] To whom correspondence should be addressed.

0021-9517/94 $6.00

flowing hydrogen (60 cc/min) for 2 h. Platinum dispersion in this catalyst was 0.87, as measured by CO chemisorption.

Samples were placed in U-tube reactors, as described previously (14). Each sample was reduced in flowing hydrogen (50 cc/min) at 673 K for 2 h, followed by evacuation (2×10^{-5} Torr) for 1 h, and cooling to room temperature. The samples were subsequently dosed with labeled ^{13}CO (99% ^{13}C, Isotech) and sealed.

All ^{13}C NMR experiments were recorded at 300 K with a Chemagnetics CMC-300 solid-state NMR spectrometer operating at 75.34 MHz. Spectra were obtained by Fourier transformation of spin echoes (90°_x–τ–180°_y–τ–acquire). The spectra shown here required 10,000–80,000 acquisitions, or 12–48 h each. All peaks are reported in parts per million (ppm) downfield from tetramethylsilane (TMS), using the carbonyl resonance of acetic acid at 178.4 ppm as a secondary reference. Spectra were deconvoluted using an iterative least-squares procedure including contributions from the following species: (1) linear CO adsorbed on diamagnetic platinum particles, a powder pattern with isotropic shift between 195 and 150 ppm, anisotropy of 260 ± 40 ppm, asymmetry fixed at 0, and Gaussian line broadening; (2) bridging CO adsorbed on diamagnetic platinum particles, a powder pattern with isotropic shift between 270 and 215 ppm, anisotropy of 110 ± 40 ppm, asymmetry between 0.1 and 0.5, and Gaussian line broadening; (3) metal-bound CO adsorbed on larger metallic platinum particles, a broad Gaussian line centered at 360 ± 20 ppm; and (4) motionally averaged CO, a Lorentzian line centered at 187 ± 20 ppm. Fits were obtained for a range of initial guesses of the shielding parameters, broadening, and fractional areas. The statistical averages are reported as the best-fit shielding parameters. The confidence limits were estimated from the variation in fits obtained with the different starting points. The relatively broad confidence ranges obtained with this procedure are quite conservative, and are preferred to the smaller values obtained from the Hessian matrix of common nonlinear least-squares analysis because of the extreme nonlinear nature of the NMR spectrum parametrization. Spin–lattice relaxation times were measured using saturation recovery and spin–spin relaxation times were measured using spin echo intensities. ^{13}C spin counts in fully relaxed spectra were typically within 5–10% of the values predicted from CO uptake measurements during sample preparation.

Infrared spectroscopy studies were conducted on a Pt/K–L-zeolite sample (ca. 0.1 g) that was pressed into a self-supporting disk (2.5 cm diameter) and placed in an IR cell fitted with CaF_2 windows. The catalyst was reduced in flowing hydrogen (100 cc/min) at 673 K for 2 h, followed by evacuation for 2 h at the same temperature. The sample was then cooled to room temperature and a background spectrum of the clean catalyst collected. A dose of carbon monoxide (Matheson), giving a coverage of ca. 20 μmol/g, was introduced into the cell at room temperature and the IR spectrum collected. Two additional doses, giving a coverage of ca. 40 μmol/g and saturation coverage with a residual gas pressure of ca. 9 Torr, were introduced and the corresponding IR spectra collected.

Infrared spectra were collected on a Nicolet FX7000 FTIR system equipped with a liquid-nitrogen-cooled MCT detector. Each spectrum was collected at 2 cm^{-1} resolution and is composed of 256 coadded scans. All spectra were collected at room temperature. The spectrum of the clean, reduced sample was used as a background reference for all spectra shown.

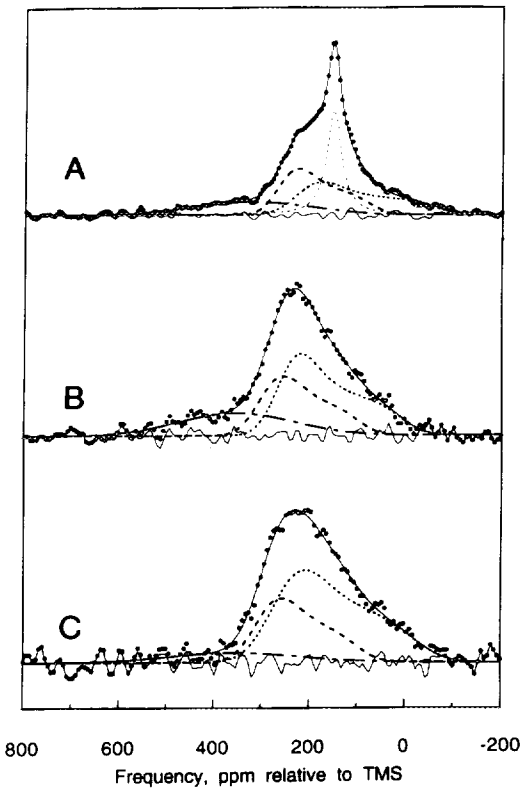

FIG. 1. ^{13}C NMR spectra of CO adsorbed on zeolite-supported Pt: (A) Pt/K–L-zeolite, under 38 Torr CO, with physisorbed CO; (B) Pt/K–L-zeolite, after evacuation, without physisorbed CO; and (C) Pt/BaK–L-zeolite, after evacuation. Each spectrum includes data and composite fit (•–•–•–•), linear CO (———) bridged CO (– – –), Knight-shifted CO (– – –), physisorbed CO (· · ·) (for spectrum a), and residual error (—). Parameters for fitted subspectra are in Table 1.

RESULTS

Carbon Monoxide Adsorbed on Pt/L-zeolites

High-resolution ^{13}C NMR spectra of CO adsorbed at saturation coverage on Pt/K–L-zeolite are shown in Fig. 1. The mean frequency of the almost fully relaxed spec-

TABLE 1

Shielding Parameters for Adsorbed CO Species

Species	Pt/K–L w/38 Torr CO				Pt/K–L after evacuation				Pt/SiO_2	
	σ^a	δ^b	η^c	w^d	σ^a	δ^b	η^c	w^d	σ^a	w^d
Linear	155	180	0	40	160	160	0	40	220	140
Bridged	226	120	0.3	30	227	122	0.35	40		
Metal-bound	360	—	—	125	360	—	—	120	360	175
Physisorbed	187	—	—	20						

[a] Isotropic shift in ppm, ±10.
[b] Shielding anisotropy in ppm, ±20.
[c] Shielding asymmetry, ±0.15.
[d] Broadening in ppm, ±20%.

trum in Fig. 1a is ca. 208 ppm. This value lies close to the range of chemical shifts observed for diamagnetic inorganic cluster compounds (22) and for CO adsorbed on supported ruthenium and rhodium (14–17). This spectrum is significantly different from the spectra of CO adsorbed on Pt/η–Al_2O_3 (10–13) and Pt/SiO_2 (10), which are Knight-shifted to 360 ppm. Qualitatively similar ^{13}C NMR spectra were obtained for both the Pt/K–L-zeolite and Pt/K(Ba)–L-zeolite catalysts. Spectra of CO adsorbed on these samples, with the gas phase evacuated, are shown in Figs. 1b and 1c.

The sharp resonance feature near 187 ppm in Fig. 1a is absent in the two latter spectra, showing that this peak is caused by physisorbed CO that is readily removed by evacuation. The NMR spectrum of CO adsorbed on a blank K–L-zeolite sample (not shown here) contains only this physisorbed component. Consequently, the sharp Lorentzian component in the spectrum of CO on Pt/K–L-zeolite arises from motionally averaged CO species that are weakly adsorbed on the zeolite framework rather than on the supported-metal particles.

The fits to spectra shown in Fig. 1 contain contributions from the following four types of adsorbed CO: linearly and bridge-bonded CO species associated with diamagnetic platinum particles, a Knight-shifted CO species located on the larger metallic platinum particles, and physisorbed CO in the zeolite. Shielding parameters and typical confidence intervals obtained by this fitting process are given in Table 1. All components included in each fit are present with statistical significance at the 99.5% confidence level. Addition of a second linearly bonded CO component or physisorbed CO in the basis set does not produce significant improvements to the fit. The chemical shift of 160 ppm for the linearly bonded CO species and the shift of 225 ppm for the bridge-bonded CO species are consistent with the ranges obtained from solution spectra of diamagnetic platinum carbonyl compounds. The linear peak is at a slightly lower frequency than usually seen. Shielding parameters used for fitting the evacuated Pt/K–L sample in Fig. 1b also fit the Pt/BaK–L sample in Fig. 1c equally well.

The infrared spectra of CO adsorbed on Pt/K–L zeolite at several coverages are shown in Fig. 2. These spectra provide the basis for including components corresponding to linearly and bridge-bonded CO species in our NMR spectral deconvolution. The infrared bands at 2067 and 1975 cm^{-1} are characteristic of linearly bonded CO and the broad band at 1760 cm^{-1} is characteristic of bridge-bonded species. As the CO pressure over the catalysts is increased, additional shoulders at 2031, 1993, and 1950 cm^{-1} are observed. These bands have been assigned to CO on platinum interacting with framework atoms in the zeolite ((8) and references therein).

Spin–spin relaxation behavior of these different sites were all comparable, as spin–echo spectral shape varied little with echo delay. T_2 values are similar for the Pt/K–L and Pt/SiO_2 samples, at 900 ± 17 and 433 ± 29 μs, respectively. For comparison, T_2 values of 450–600 μs

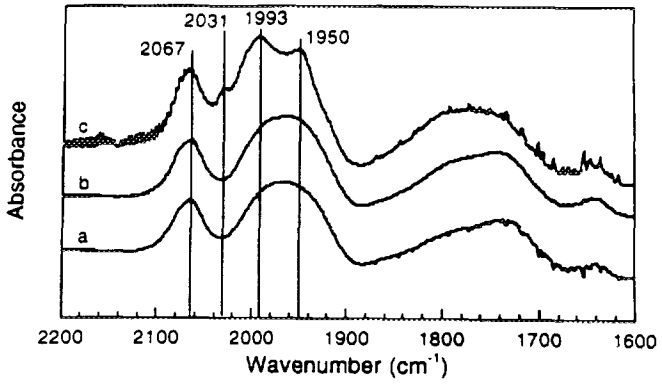

FIG. 2. IR spectra of CO adsorbed on 1% Pt/K–L-zeolite: (a) at ca. 20 μmol/g CO coverage, (b) at ca. 40 μmol/g CO coverage, and (c) at saturation coverage under 9 Torr of CO.

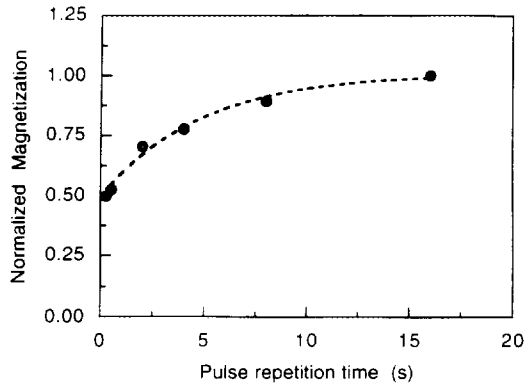

FIG. 3. Room temperature saturation-recovery behavior for CO on 1% Pt/K–L zeolite after evacuation (sample sealed under 38 Torr of ^{13}CO).

for CO adsorbed on diamagnetic rhodium particles supported on SiO_2 (16) and 800 μs for CO adsorbed on Pt/η–Al_2O_3 (26) have been reported. Second-moment calculations predict T_2 of 1200–800 μs for sites on a planar surface with 3–6 CO neighbors at a close-packed distance of 3.2 Å. Thus, the T_2 values seen for CO/Pt here indicate that ^{13}C–^{13}C dipolar coupling contributes significantly to spin–spin relaxation and that the CO surface density is close to that on other metal surfaces and on Pt supported on other supports. The slight decrease in relaxation rate indicated by the longer relaxation time on the Pt/K–L sample points to either a decrease in the number of CO neighbors or to an increase in the ^{13}C–^{13}C distance. Both of these results are consistent with the presence of smaller particles with high surface curvature in the Pt/K–L sample. The faster spin–spin relaxation rate seen for the Pt/SiO_2 sample indicates contributions from other relaxation sources, the most significant of which is the coupling of the ^{13}C spins with conduction electron spins in the metallic platinum particles (*vide infra*).

Differences in relaxation times can be used to evaluate the separate contributions of various species in an NMR spectrum. Saturation–recovery integrated peak area relaxation data are shown in Fig. 3 for the Pt/K–L sample under 38 Torr CO. The recovery of magnetization is nonexponential, indicating contributions from several relaxation times. A period of rapid recovery is followed by a period of slow recovery. Nearly 45% of the total magnetization has recovered by 0.25 s, indicating the presence of rapidly relaxing components. Spectra collected with short pulse repetition times have relatively more intensity in the Knight-shifted and physisorbed CO peaks than in the diamagnetic species. Spectra collected at longer pulse repetition times include contributions from all adsorbed species. Each of these partially relaxed spectra can be decomposed into a sum of contributions using the basis functions shown above, and saturation-recovery relaxation fits to these intermediate spectra (which produced the data points in Fig. 3) allow estimation of individual T_1 values for each site. With this approach, the physisorbed CO and the Knight-shifted CO are both seen to have T_1 values below 0.1 s, while the linear and bridging CO on diamagnetic Pt particles have relaxation times of up to 6 s. Table 2 presents the T_1 values for each species in these samples, along with the fractional area each contributes to a fully relaxed spectrum.

The disparate relaxation rates seen for different spectral components confirm that they are indeed separate species. The linear and bridge-bonded CO have longer time constants and relax at different rates, in contrast to CO on other small catalyst particles (16). The physisorbed CO relaxes extremely rapidly, consistent with fast motion between weakly adsorbed sites. The sample with physisorbed CO displays reduced T_1 values for linear and bridged CO on Pt particles, as well.

A sealed, spinnable sample of the Pt/K–L-zeolite catalyst was also prepared, and its spectrum is presented in Fig. 4. Magic-angle sample spinning (MAS) averages the chemical shift anisotropy interaction to produce a family of sharp peaks for each well-defined species, improving spectral resolution and providing additional information. In this spectrum, sharp isotropic peaks are observed at 123, 157, and 168 ppm. Spectra obtained at other spinning speeds showed the other peaks to be spinning sidebands. The peak at 123 ppm is a CO_2 impurity, probably introduced during the sealing process. The peaks at 157 and 168 ppm, along with their associated spinning sidebands, are consistent with the shielding parameters obtained above for linear CO. The two isotropic peaks indicate that the single linear tensor used in the wideline fits is actually an average of two well-defined sites, as might be seen for edge and corner CO sites. There are no sharp peaks produced by the bridging CO, although the broad roll in the baseline from 300–100 ppm shows that the intensity remains in a broad peak instead of averaging into spinning sidebands. This inability to detect bridging CO with MAS is common, and has been attributed to bridging CO populating a variety of geometries with a range of isotropic shifts and thus not narrowing into a single spinning sideband family (17).

Carbon Monoxide Adsorbed on Pt/SiO_2

Catalysts consisting of platinum supported on silica and alumina typically have particles that are sufficiently large to have a well-developed conduction band (10–13). The interaction of electrons in this conduction band with electrons in the molecular orbitals of adsorbed CO leads to a broad, Knight-shifted resonance in the ^{13}C NMR spectrum that appears 200 ppm downfield from the chemical-shift

TABLE 2

Relaxation Parameters for Adsorbed CO Species

Species	Pt/K–L w/38 Torr CO		Pt/K–L after evacuation		Pt/SiO_2	
	(% area)	T_1(s)	(% area)	T_1(s)	(% area)	T_1(s)
Linear	32 ± 1	0.24 ± 0.03	50 ± 3	1.5 ± 0.3	23 ± 2	2.6 ± 0.7
Bridged	35 ± 1	2.2 ± 0.2	36 ± 4	6.6 ± 1.6		
Metal-bound	14 ± 1	0.36 ± 0.09	14 ± 2	0.8 ± 0.6	77 ± 2	0.0 ± 0.01
Physisorbed	19 ± 1	0.01 ± 0.01				

values observed for CO ligands in diamagnetic organometallic cluster compounds (22).

The ^{13}C NMR spectra of CO adsorbed on 4% Pt/SiO_2 display a single broad peak that shifts from 360 to 320 ppm as the pulse repetition time increases. A typical spectrum, for a recycle delay of 2 s, is presented in Fig. 5 and the saturation–recovery data for this system are shown in Fig. 6. As with the Pt/K–L-zeolite system, the recovery of magnetization is nonexponential, indicating a distribution of T_1 relaxation times. The saturation–recovery data can be fit by two exponentials. The shift in the center of spectrum as a function of pulse repetition time illustrates that the slowly relaxing components arise from CO species that resonate at higher fields.

In agreement with previous studies, we assign the rapidly relaxing components to Knight-shifted CO species resonating at low fields. This peak is centered at 360 ppm in the Pt/SiO_2 sample and all other samples studied here. In addition, we propose that the slowly relaxing components correspond to CO species resonating at chemical-shift values typical of diagmagnetic platinum particles. Fitting the full set of saturation–recovery spectra to two species with Gaussian lines as described in Table 1 results in the parameters shown in Table 2. Similar results are obtained using a linear CO tensor centered at 160 ppm, but use of the additional parameters required to describe this or a bridging CO tensor is not statistically justified for this data set. The relaxation time for the Knight-shifted CO is less than 10 ms, while the diamagnetic CO peak has a T_1 of 2.6 s. Figure 5 shows a nearly relaxed ^{13}C NMR spectrum of CO adsorbed on 4% Pt/SiO_2 from a long acquisition, along with a spectral deconvolution. The fit indicates that 90% of the CO is Knight-shifted and 10% is diamagnetic, in agreement with the behavior expected for a spectrum collected with a 2-s recycle delay from the T_1 and fractional area values determined above.

DISCUSSION

This work shows an extension of ^{13}C NMR of adsorbates as a probe of metal particle properties. Bradley *et al.* (23) have recently reported a study of CO ligands

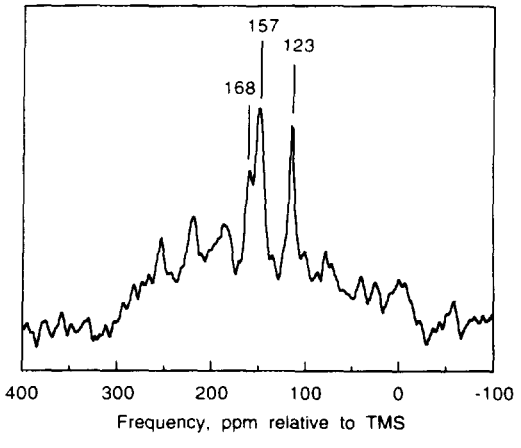

FIG. 4. Magic-angle spinning spectrum (2.6 kHz, resolution of 0.8 ppm/point) of CO on Pt/K–L-zeolite after evacuation. Labeled peaks are isotropic peaks, and remaining peaks are spinning sidebands.

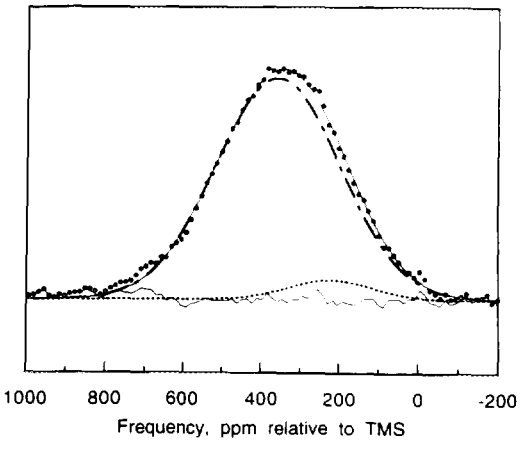

FIG. 5. ^{13}C NMR spectrum of CO adsorbed on 4% Pt/SiO_2. Parameters for fitted subspectra are in Table 1. Spectral decomposition shows diamagnetic (····) and Knight-shifted (– – – –) species.

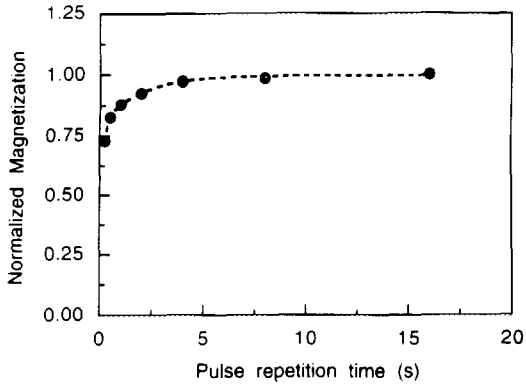

FIG. 6. Room-temperature saturation recovery data for CO adsorbed on 4% Pt/SiO_2.

on highly dispersed colloidal platinum and palladium particles, where a broad ^{13}C NMR peak centered at 194 ppm was observed for CO adsorbed on colloidal platinum particles smaller than 0.8 nm and a ^{13}C NMR shift of 190 ppm was observed for colloidal palladium particles smaller than 2.0 nm. These authors also showed that CO adsorbed on colloidal palladium larger than 7.0 nm were significantly Knight shifted (24). In a similar manner, the NMR spectra of CO adsorbed on poorly dispersed Rh particles are broad and ill-defined, while spectra for highly dispersed samples are well-defined and dominated by contributions from diamagnetic species (14, 15). It has been suggested that the transition from well-defined powder patterns to the broad Lorentzian or Gaussian peaks seen for Knight-shifted CO may be a useful indicator of the change from diamagnetic to metallic behavior (18).

The NMR spectroscopy results reported in the present paper are in agreement with the finding by Vaarkamp *et al.* (9) that the Pt particles in this Pt/K–L-zeolite sample consist of 5–6 atoms. These Pt clusters are unlikely to possess a fully developed conduction band and will not contribute to Knight-shift interactions in the ^{13}C NMR spectrum.

Knight Shift Onset

The frontier orbitals in a small metal particle will begin to behave like a conduction band in an NMR experiment and generate a Knight shift when the electronic energy levels are spaced closely enough. This occurs when the ESR level spacing and thermal energy are sufficient to promote an electron with its spin antiparallel to the external magnetic field to an unoccupied energy level with spin parallel to the magnetic field. This electron polarization causes a relative increase of 10^{-3} in the field strength as detected by NMR. However, since local field variations caused by orbital electronic shielding are normally 10–100 ppm, the Knight shift of 1000–10,000 ppm is a large effect. The polarized or unpaired electrons also produce fluctuating magnetic fields that broaden the NMR peak and greatly increase relaxation rates, so T_1 values in metals are typically 1 ms or less. A species adsorbed on a metal particle, such as CO, will experience some of the polarization of metallic electrons from donor bond and back-bond interactions.

For these Pt particles, we can readily estimate the particle size where this overlap begins. Based on the Pt heat of vaporization, the Pt–Pt bond energy is approximately $\Delta E = 22.5$ kcal/mole. In an n-atom particle, the electronic energy level spacing will be proportional to $\Delta E/n$. Electron spin interaction with the 7 Tesla magnetic field shifts the spin-up and spin-down manifolds by 200 GHz, or $E_s = 20$ cal/mole, and at 300 K thermal energy broadens the Fermi distribution function to cover roughly $kT = 600$ cal/mole. An order of magnitude estimate indicates that electron promotion and polarization become significant for a Pt particle containing $n = 36$ atoms, where $n = \Delta E/(E_s + kT)$. This crude estimate justifies the NMR-based Pt particle size descriptions proposed above. The 5–6 atom clusters in zeolite cavities with energy levels ~4 kcal/mole ($= \Delta E/n$) apart will be well below the onset of metallic behavior, while Pt particles outside the zeolite crystallites with >100 atoms and energy levels ~200 cal/mol apart will have metallic character. A more detailed model incorporating actual density of states (DOS) information would correctly predict that Knight-shifted behavior would occur for smaller particles of Pd and Pt, and only at larger particle sizes for Ru and Rh, since Pd and Pt have been shown to have the highest DOS of the noble metals (25).

The small fraction of platinum particles that are large enough to display Knight-shifted spectra must be outside the zeolite crystallite, and are often observed by electron microscopy. In this respect, the relative amount of diamagnetic versus Knight-shifted CO adsorbed on platinum can, therefore, be used as an analytical tool to determine the fraction of the Pt surface sites that are associated with Pt clusters within the zeolite framework. It is noteworthy that the formation of cluster-sized particles within L-zeolite is widely described as a prerequisite for the catalyst to exhibit high aromatization activity, selectivity, and stability.

Relaxation Behavior

The NMR spectra observed in the present study of CO adsorbed on Pt/SiO_2 are dominated by a Knight-shifted component associated with CO on platinum particles large enough to display metallic behavior. The spectrum shown in Fig. 5 is qualitatively similar to the spectra of CO adsorbed on Pt/η–Al_2O_3 observed by Slichter and coworkers (10–13) and by Zilm *et al.* (26). Slichter and

co-workers report that on a $Pt/\eta-Al_2O_3$ catalyst with a dispersion of 76%, the relaxation at 77 K is nonexponential and can be fit to a set of three exponentials with relaxation times of 0.009, 0.3, and 6.0 s. As a result of CO diffusion on the surface of the metal particles, the relaxation data at 300 K can be fit by a single relaxation time of 0.130 s. Similarly, Zilm *et al.* report an average relaxation time of 0.135 s for CO adsorbed on $Pt/\eta-Al_2O_3$ catalyst having a dispersion of 80%. Our relaxation measurements and shift values for the fast-relaxing component are in excellent agreement with these observations reported in previous studies.

The nonexponential relaxation behavior observed for CO on our Pt/SiO_2 catalyst might be intepreted instead as a result of incomplete averaging of relaxation rates due to hindered diffusion over the particle faces. However, the average T_1 of 0.10 s obtained for the fast-relaxing component at 360 ppm on our catalyst is in excellent agreement with the values reported by the other studies, indicating that diffusion has already served to average all relaxation rates on the Knight-shifted particles.

The spectrum obtained using long pulse repetition times for CO on Pt/SiO_2 at 298 K is qualitatively similar to the spectrum obtained with the shortest repetition time. However, the mean chemical shift of these spectra decreases with increasing repetition times, indicative of increasing intensity from components shifted to higher field. This trend could arise either from anisotropic relaxation across the Knight-shifted component or from a separate component relaxing slowly at high field. The relaxation data on our catalysts, however, show that the slowest of the Knight-shifted components should have completely relaxed by ca. 0.85 s. Therefore, we believe that the slowly relaxing component that resonates at high field for CO on Pt/SiO_2 arises from a separate species not connected with the Knight-shifted component. The isotropic shift of this separate species falls within the range of shifts observed for linearly and bridge-bonded CO on diamagnetic platinum clusters (27, 28) and also for CO adsorbed on supported rhodium and ruthenium catalysts (14–17).

More importantly, the mean chemical shift and relaxation times for this slow-relaxing component agree with data for the Pt/K–L system, which consists primarily of diamagnetic platinum particles. Accordingly, we propose that the small amount (ca. 20%) of slowly relaxing component resonating at diamagnetic shift ranges for CO on 4% Pt/SiO_2 arises from CO adsorbed on Pt particles small enough to display nonmetallic behavior. These cluster-sized particles on SiO_2 may be present from the ion-exchange procedure used to prepare the catalyst. Finally, the Knight-shifted particles on the Pt/SiO_2 catalysts used here or described by others (10–13) are still small and the dispersions are not very different from those reported for diamagnetic Rh or Ru particles (14–19). This behavior is consistent with our conclusion in the previous section that the critical particle size for development of a conduction band varies depending on the metal used, with Pt and Pd developing conduction bands and strong Knight-shifted CO at smaller particle sizes than Rh and Ru.

Comparisons of the spectra for Pt/K–L and Pt/K–Ba–L zeolites reveal several other interesting features. First, the K–L sample shows a small peak (14% of adsorbed CO) for Knight-shifted Pt sites, with the Ba-exchanged sample exhibiting only 9% of CO adsorbed on large, metallic Pt particles. Within the limits of the fit uncertainties, this difference may indicate that the addition of Ba improves stability of small Pt particles in zeolite cavities or suppresses formation of large Pt particles on the crystallite exterior, and it is consistent with the observed improvement of catalyst behavior on inclusion of Ba. Second, the linear : bridge ratio for the Ba-containing catalyst is substantially larger than that for the Pt/K–L sample (2 : 1 versus 3 : 2, respectively), which may also indicate that addition of Ba results in smaller Pt particles.

The linear and bridged CO on intrazeolite Pt particles have substantially different spin-lattice relaxation rates. In contrast, on Rh or Ru particles the linear and bridged CO showed a common T_1 value. This difference can be examined in light of the different characteristics of the common relaxation mechanisms. Motion of the metal particle would give T_1 values proportional to the chemical shielding anisotropy (CSA), wagging and reorientation of individual CO molecules would give relaxation dependent on both CSA and libration extent, and interactions with paramagnetic sites (support impurities) would produce a common relaxation rate for all sites. The latter effect dominated for Rh or Ru particles on SiO_2, but none of these mechanisms can produce the factor of 4 difference observed for Pt/K–L zeolites. In consideration of the size of a 5–6 Pt atom particle with adsorbed CO, we may assume that the linear CO molecules at edge and corner sites interact more strongly with the walls of the zeolite cavity than does the bridging CO, which projects less far from the particles. Pt-particle motion, collision with walls, or other fluctional interactions could produce larger magnetic field fluctuations for linear CO, hastening its relaxation.

The decrease in relaxation times for linear and bridging CO when physisorbed CO is present may be due to slow exchange or dipole–dipole interactions between these species. The possibility of exchange is supported by the increase in linewidth of physisorbed CO from 4 ppm on the blank zeolite to 40 ppm on the Pt-exchanged zeolite. The greater reduction in the relaxation time for linear CO and decrease in its relative area in the presence of physisorbed CO suggests that physisorbed CO exchanges much more rapidly with linear CO than bridged CO.

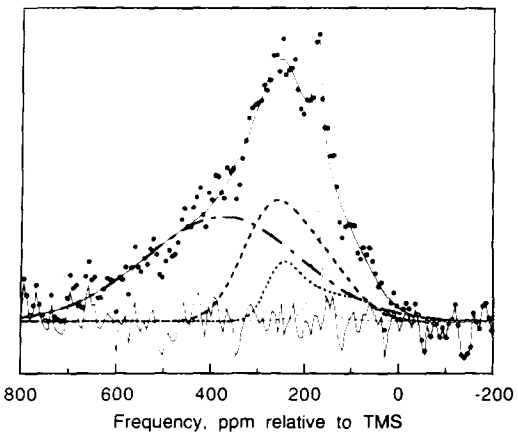

FIG. 7. ^{13}C NMR spectrum of CO adsorbed on less-optimized Pt/K–L-zeolite catalyst. Subspectra are keyed as in Fig. 1.

Catalyst Screening Application

One of the objectives in the preparation of Pt/zeolite catalysts is to stabilize small Pt particles in the zeolite channels. It has been observed that smaller particles inside the zeolite channels are more selective for dehydrocyclization, less selective for hydrogenolysis and deactivate less compared to larger particles supported on the external surface. Since the size and location of the Pt particles depend strongly on the mode of preparation and subsequent treatment procedures (29), a quantitative evaluation of the Pt particle size appears useful in screening and characterizing these catalysts.

The results presented above show that ^{13}C NMR of chemisorbed CO has the potential to quantify and distinguish between large and small Pt particles. To explore this potential use, spectra were collected for CO adsorbed on another Pt–K–L zeolite catalyst of lower dispersion. The result, shown in Fig. 7, indicates that the same CO chemisorption sites are present in different proportions. The CO site fractions are linear : bridge : Knight-shifted = 0.1 : 0.3 : 0.5, with a trace of physisorbed CO also shown. Indeed, this catalyst preparation produced significantly more of the Pt as large particles outside the zeolite framework than was seen for the more highly optimized samples used for Fig. 1. Thus, this catalyst would be expected to be less selective for hexane aromatization.

CONCLUSIONS

The ^{13}C NMR spectrum of CO adsorbed on 4% Pt/SiO_2 is composed primarily of a Knight-shifted peak, with a small contribution from CO adsorbed on diamagnetic platinum particles. The adsorption of CO on platinum supported in L-zeolite leads to a well-resolved ^{13}C NMR spectrum dominated by diamagnetic species. This spectrum can be described by contributions from linear- and bridge-bonded CO associated with the diamagnetic platinum clusters, Knight-shifted CO species associated with particles large enough to display metallic behavior, and CO species physisorbed on the zeolite. These results indicate that platinum in L-zeolite is present primarily as cluster-sized particles that do not possess a fully developed conduction band. Furthermore, ^{13}C NMR is shown to allow quantitative detection and characterization of the CO adsorption sites present on these small particles in the zeolite pores.

The ratio of diamagnetic to Knight-shifted components in the ^{13}C NMR spectrum of Pt/L catalysts can be used to determine the fractions of the Pt surface associated with Pt clusters in the channels of L-zeolite or with larger Pt particles located on the external surface of the zeolite. In addition, the ability to collect solid-state ^{13}C NMR spectra that are not dominated by the Knight shift allows ^{13}C NMR to be used to provide unique information about the nature of carbon-containing species on platinum surfaces.

ACKNOWLEDGMENTS

We acknowledge the donors of the Petroleum Research Fund, administered by the American Chemical Society, for partial support of this research. This research was also supported in part by NSF Grants CBT-8657496 and CTS-9123197. In addition, we are grateful to Dr. Randy Cortright for assistance with catalyst preparation.

REFERENCES

1. Bernard, J. R., *in* "Proceedings, 5th International Conference on Zeolites," p. 686. Heyden, London, 1980.
2. Besoukhanova, C., Breysse, M., Bernard, J. R., and Barthomeuf, D., *in* "Catalyst Deactivation," Stud. Surf. Sci. Catal. (B. Delmon and G. F. Froment, Eds.), Vol. 6, p. 201 Elsevier, Amsterdam, 1980.
3. Besoukhanova, C., Breysse, M., Bernard, J. R., and Barthomeuf, D., *Stud. Surf. Sci. Catal. B* (New Horizons in Catalysis) **7**, 1410 (1981).
4. Besoukhanova, C., Guidot, J., and Barthomeuf, D., *J. Chem. Soc., Faraday Trans.* **77**, 1595 (1981).
5. Hughes, T. R., Buss, W. C. Tamm, P. W., and Jacobson, R. L., Studies in Surface Science and Catalysis, Proc. 7th Inter. Zeolite Conf., New Developments in Zeolite Science and Technology, ed. Y. Murakami, A. Iijima, and J. W. Ward. Vol. 28, Elsevier, Amsterdam, 1986.
6. Tamm, P. W., Mohr, D. H., and Wilson, C. R., T-4, *in* "Catalysis 1987, Studies in Surface Science and Catalysis, Proc. 10th North American Meeting of the Catalysis Society" (B. Delmon and J. T. Yates, Eds.), p. 335. North American Catalysis Society, New York, 1988.
7. Larsen, G. and Haller, G. L., *Catal. Lett.* **3**, 103 (1989).
8. Hicks, R. F., Han, W. J., and Kooh, A. B., *in* "Proceedings, 10th International Congress on Catalysis, Budapest, 1992" (L. Guczi, F. Solymosi, and P. Tetenyi, Eds.), p. 167. Akadémiai Kiadó, Budapest, 1993.
9. Vaarkamp, M., Grondelle, J. V., Miller, J. T., Sajkowski, D. J., Modica, F. S., Lane, G. S., Gates, B. C., and Koningsberger, D. C., *Catal. Lett.* **6**, 369 (1990).

10. Ansermet, J. Ph., Slichter, C. P., and Sinfelt, J. H., *J. Chem. Phys.* **88**(9), 5963 (1988).
11. Ansermet, J. Ph., Wang, P. K., Slichter, C. P., and Sinfelt, J. H., *Phys. Rev. B: Condens. Matter* **37**(4), 1417 (1988).
12. Rudaz, S. L., Ansermet, J. Ph., Wang, P. K., Slichter, C. P., and Sinfelt, J. H., *Phys. Rev. Lett.* **54**(1), 71 (1985).
13. Wang, P. K., Ansermet, J. Ph., Rudaz, S. L., Wang, Z., Shore, S., Slichter, C. P., and Sinfelt, J. H., *Science* **234,** 35 (1986).
14. Duncan, T. M., Yates, J. T., Jr., and Vaughan, R. W., *J. Chem. Phys.* **73**(2), 975 (1980).
15. Duncan, T. M., Yates, J. T., Jr., and Vaughan, R. W., *J. Chem. Phys.* **71**(7), 3129 (1979).
16. Duncan, T. M. and Root, T. W., *J. Phys. Chem.* **92**(15), 4426 (1988).
17. Duncan, T. M., Zilm, K. W., Hamilton, D. M., and Root, T. W., *J. Phys. Chem.* **93**(6), 2583 (1989).
18. Duncan, T. M., *Colloids Surf.* **45,** 11 (1990).
19. Compton, D. B., Ph.D. Dissertation, University of Wisconsin-Madison, 1991.
20. Sharma, S. B., Ouraipryvan, P., Nair, H. A., Balaraman, P., Root, T. W., and Dumesic, J. A., *J. Catal.* **150,** 234 (1994).
21. Benesi, H. A., Curtis, R. M., and Studer, H. P., *J. Catal.* **10,** 328 (1968).
22. Gleeson, J. W. and Vaughan, R. W., *J. Chem. Phys.* **78**(9), 5384 (1983).
23. Bradley, J. S., Millar, J. M., Hill, E. W., and Behal, S., *J. Catal.* **129,** 530 (1991).
24. Bradley, J. S., Millar, J. M., Hill, E. W., and Melchoir, M., *J. Chem. Soc., Chem. Commun.* **705,** (1990).
25. Gladstone, G., Jensen, M. A., and Schrieffer, J. R., *in* "Superconductivity," Vol. 1, p. 665. (R. D. Parks, Ed.), Dekker, New York, 1969.
26. Zilm, K. W., Bonneviot, L., Hamilton, D. M., Webb, G. G., and Haller, G. L., *J. Phys. Chem.* **94,** 1463 (1990).
27. Washecheck, D. M., Wucherer, E. J., Dahl, L. F., Ceriotti, A., Longoni, G., Manassero, M., Sansoni, M., and Chini, P., *J. Am. Chem. Soc.* **101,** 6110 (1979).
28. Chisholm, M. H., Clark, H. C., Manzer, L. E., Stothers, J. B., and Ward, J. E. H., *J. Am. Chem. Soc.* **95,** 8574 (1973).
29. Ostgard, D. J., Kustov, L., Poeppelmeier, K. R., and Sachtler, W. M. H., *J. Catal.* **133,** 342 (1992).